nature geoscience

LETTERS

PUBLISHED ONLINE: 18 JANUARY 2016 | DOI: 10.1038/NGEO2622

Massive and prolonged deep carbon emissions associated with continental rifting

Hyunwoo Lee[1]*, James D. Muirhead[2], Tobias P. Fischer[1], Cynthia J. Ebinger[3], Simon A. Kattenhorn[2,4], Zachary D. Sharp[1] and Gladys Kianji[5]

Carbon from Earth's interior is thought to be released to the atmosphere mostly via degassing of CO_2 from active volcanoes[1–4]. CO_2 can also escape along faults away from active volcanic centres, but such tectonic degassing is poorly constrained[1]. Here we use measurements of diffuse soil CO_2, combined with carbon isotopic analyses to quantify the flux of CO_2 through fault systems away from active volcanoes in the East African Rift system. We find that about 4 Mt yr^{-1} of mantle-derived CO_2 is released in the Magadi–Natron Basin, at the border between Kenya and Tanzania. Seismicity at depths of 15–30 km implies that extensional faults in this region may penetrate the lower crust. We therefore suggest that CO_2 is transferred from upper-mantle or lower-crustal magma bodies along these deep faults. Extrapolation of our measurements to the entire Eastern rift of the rift system implies a CO_2 flux on the order of tens of megatonnes per year, comparable to emissions from the entire mid-ocean ridge system[2,3] of 53–97 Mt yr^{-1}. We conclude that widespread continental rifting and super-continent breakup could produce massive, long-term CO_2 emissions and contribute to prolonged greenhouse conditions like those of the Cretaceous.

Emissions of mantle-derived CO_2 are thought to be sourced primarily at volcanic centres, where it is currently estimated that ~90% of Earth's natural CO_2 is released through active degassing of volcanic plumes or passive, diffuse emissions around volcanic edifices, mid-ocean ridges, and volcanic lakes[1–4]. One major source of discrepancy in global flux estimates relates to sparse sampling of diffuse CO_2 flux in fault systems away from volcanic centres[5]. These areas of tectonic degassing (for example, the Apennines, Italy; ref. 6) exhibit high surface CO_2 fluxes sourced from deep magma bodies, yet have no expression of recently active volcanism (such as composite volcanoes or calderas, see Supplementary Information). Although magma-rich continental rifts (for example, the East African and Rio Grande rifts) represent prime targets to test and quantify this mode of CO_2 transfer, gross estimates of CO_2 flux within areas of tectonic degassing are currently restricted to only a few localities globally (Italy and the Pacific Rim; refs 5,6). Consequently, global CO_2 flux from natural systems is likely to be underestimated[5].

The East African Rift (EAR) is the world's largest active continental rift, comprising distinct western and eastern sectors with a cumulative length of >3,000 km (ref. 7). Active volcanoes in the EAR, such as Nyiragongo (≥3.4 Mt yr^{-1}; ref. 8) and Oldoinyo Lengai (2.42 Mt yr^{-1}; ref. 9), emit large volumes of CO_2 and significant amounts of CO_2 are stored in large anoxic lakes (for example, Lake Kivu; ref. 10). Fault systems dissecting active volcanic centres in the EAR (such as the Aluto complex, Ethiopia) have been shown to provide local pathways through which CO_2-rich fluids are transported from shallowly degassing magma chambers[11]. However, earthquake swarms spanning the crustal depth range, interpreted as the release and rise of CO_2-rich fluids through faults, are also observed in EAR basins away from active volcanic centres (for example, Albertine basin; ref. 12). Despite these findings, no study has tested the volumetric capacity of rift-wide fault systems in the EAR to transport deeply derived CO_2. Here we provide strong evidence that significant volumes of CO_2, probably sourced from upper mantle and/or lower crustal magma bodies, are emitted through fault systems positioned away from active volcanic centres in the EAR.

The volume of CO_2 released diffusively at any volcanic-tectonic setting can be estimated from soil CO_2 flux measurements, whereas CO_2 sources (mantle and/or biogenic, for example) may be characterized by carbon isotope compositions[13,14]. We investigated diffuse CO_2 emissions within fault populations in the Magadi–Natron basin at the Kenya–Tanzania border (Fig. 1 and Table 1). Diffuse CO_2 flux was measured with an accumulation chamber[13] at the base of fault scarps (termed here fault zones) and compared with background values in hanging walls and footwalls across horst and graben structures (see Supplementary Information). Gas samples were collected by diverting gas from the chamber into pre-evacuated glass vials during flux measurements[15]. These samples were analysed in the laboratory for $\delta^{13}C$-CO_2 (‰) and CO_2 concentrations, and compared with samples collected on Oldoinyo Lengai, an active volcano at the southern terminus of the Natron basin (Fig. 1a). Seismicity data were collected on the 38-station CRAFTI broadband seismic array (see Methods).

Carbon isotope compositions indicate a strong mantle contribution to the observed CO_2 (Fig. 2). Measured $\delta^{13}C$-CO_2 values range from −3.8 to −11.7‰ with a mean value of −8.0 ± 1.3‰ (Table 1), and 78% of values fall within the mantle range (−6.5 ± 2.5‰; ref. 16). All $\delta^{13}C$-CO_2 values are distinctively heavier than biogenic $\delta^{13}C$ values from soil CO_2 studies along transform plate boundaries elsewhere, such as the San Andreas fault (−21.6 to −23.7‰; ref. 14). Although two samples have similar $\delta^{13}C$-CO_2 values (−3.8‰ and −4.3‰, respectively) to fumaroles on Oldoinyo Lengai volcano (−2.36 to −4.01‰; ref. 17), they are within the range of isotope values from mantle-derived CO_2 collected in volcanic and geothermal areas in the Kenya rift

[1]Department of Earth and Planetary Sciences, University of New Mexico, Albuquerque, New Mexico 87131-0001, USA. [2]Department of Geological Sciences, University of Idaho, Moscow, Idaho 83844-3022, USA. [3]Department of Earth and Environmental Sciences, University of Rochester, Rochester, New York 14627, USA. [4]ConocoPhillips, Houston, Texas 77079, USA. [5]Department of Geology, Chiromo Campus, University of Nairobi, PO Box 30197-00100, GPO Nairobi, Kenya. *e-mail: lhw615@unm.edu

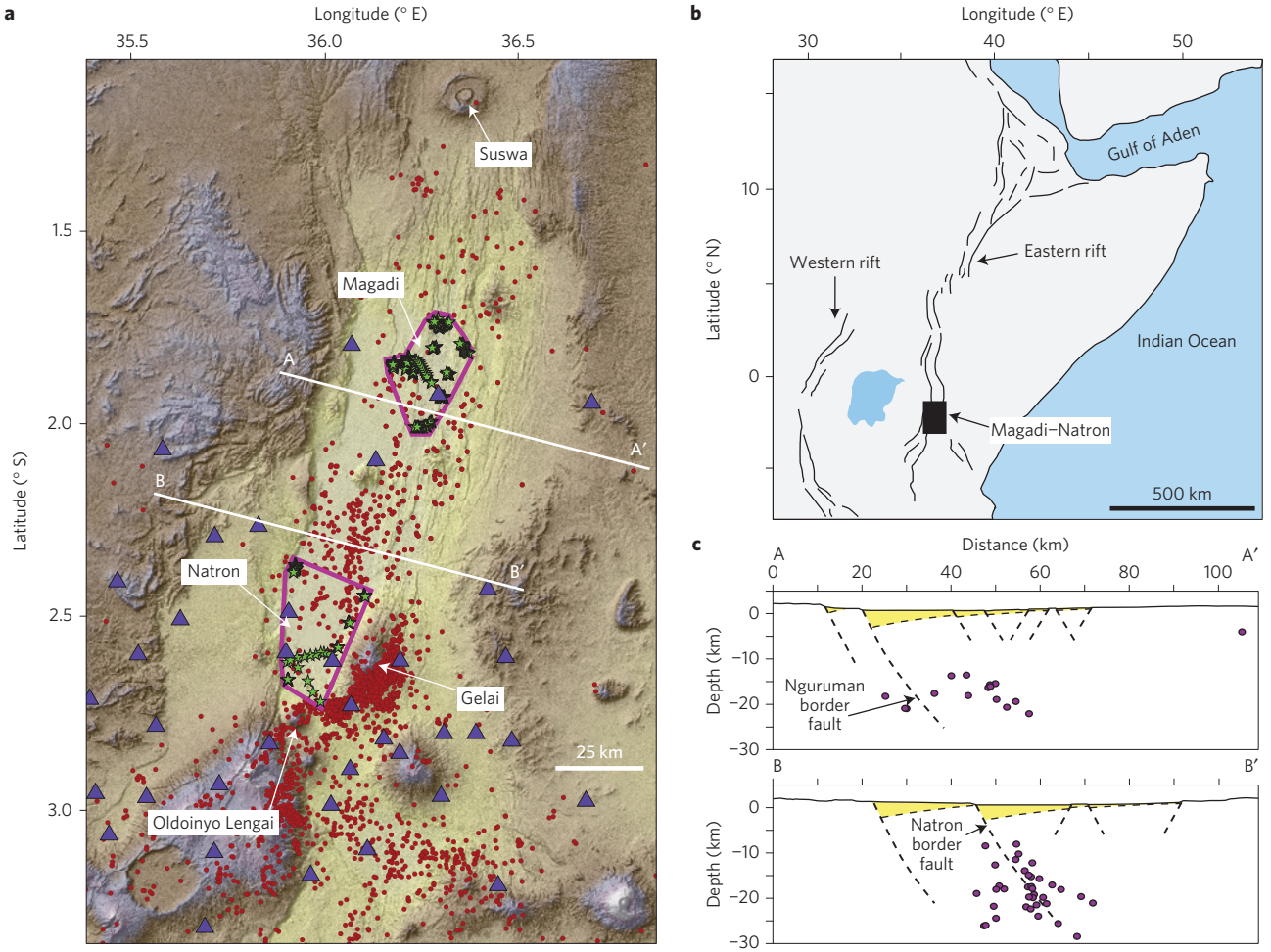

Figure 1 | Distribution of CO_2 flux samples and seismicity. a, SRTM map of the Magadi–Natron basin. Active volcanic centres (Suswa, Gelai, and Oldoinyo Lengai) are annotated. Green stars show CO_2 measurement locations. Red circles show earthquake epicentres from the CRAFTI seismic network (purple triangles). **b**, Location of the study area. **c**, Cross-sections from A–A′ and B–B′ in **a**. Purple circles represent earthquake foci 2 km from each section. Yellow fill represents basin sediments[20,21]. Border faults are projected to lower crustal seismicity using surface and seismic observations.

Table 1 | CO_2 fluxes, mean CO_2 concentrations and $\delta^{13}C$ from the Magadi–Natron basin.

	Area (km^2)	Mean flux ($g\,m^{-2}\,d^{-1}$)	Total flux ($t\,d^{-1}$)	Annual flux ($Mt\,yr^{-1}$)	CO_2 (ppm)	$\delta^{13}C - CO_2$ (‰ versus PDB)
Magadi						
Fault zones	72.9	36.6 ± 11.0	2,672 ± 804	0.98 ± 0.29	1,056 ± 581	−7.8 ± 1.3
Background	334.6	4.9 ± 1.9	1,650 ± 649	0.61 ± 0.24	789 ± 209	−8.1 ± 1.4
Sum	407.5		4,327 ± 1,453	1.59 ± 0.53		
Natron						
Fault zones	33.1	17.2 ± 5.0	570 ± 166	0.21 ± 0.06	944 ± 158	−8.1 ± 2.0
Background	540.9	11.4 ± 6.6	6,176 ± 3,592	2.25 ± 1.31	837 ± 108	−8.5 ± 1.3
Sum	574.0		6,746 ± 3,758	2.46 ± 1.37		
Total	981.5			4.05 ± 1.90	929 ± 386	−8.0 ± 1.3

Fluxes are ± 95% confidence. Mean values of CO_2 concentrations and $\delta^{13}C$ are $\pm 1\sigma$. Fault zones occur adjacent to fault scarps, extending outward on the downthrown side a distance equal to the maximum throw. Faults were mapped from aerial photos and throws were estimated using a measured throw/length ratio of 0.0061. Background values represents the combined CO_2 flux from hanging walls (downthrown sediments) and footwalls (uplifted lavas) measured from aerial photos and LandSat imagery, and validated in the field. See also Supplementary Information (Supplementary Fig. 1 and Supplementary Table 3).

(−1.7 to −6.9‰; ref. 18). CO_2 concentrations of our samples (<0.4%; Supplementary Table 1) are lower than typical magmatic and hydrothermal gases (0.5–11.9%; ref. 19), which may be attributed to dilution of mantle-derived CO_2 by air during diffuse degassing (Fig. 2). For example, following the approach of ref. 15, plots of $\delta^{13}C$ and CO_2 concentrations fit on a mantle–air mixing line (Fig. 2). Samples with lighter $\delta^{13}C$ values (<−9‰) are possibly affected by minor contributions of biogenic CO_2 to a predominantly mantle-derived CO_2 and air mixture.

An elevated CO_2 flux in fault zones of the Magadi–Natron basin (Table 1; Fig. 3) provides strong evidence that faults act as permeable pathways that facilitate the ascent of the deeply derived CO_2 (see also Supplementary Information). Mean values of diffuse CO_2 flux in fault zones of the Magadi and Natron study areas

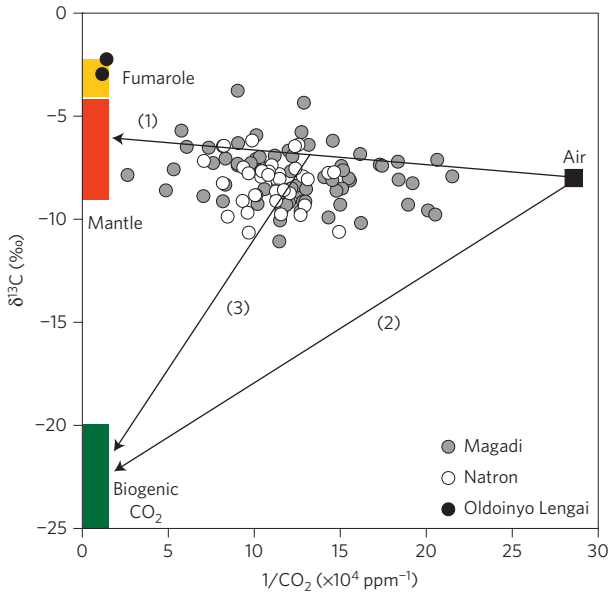

Figure 2 | Carbon isotope compositions and concentrations of diffuse CO_2 in the Magadi–Natron basin. $\delta^{13}C$-CO_2 versus the reciprocal of CO_2 concentration. Mantle $\delta^{13}C$ values (red box) are -6.5 ± 2.5‰ (ref. 16). $\delta^{13}C$ values of fumaroles (yellow bar) are from ref. 17. Biogenic CO_2 (green bar) ranges from -20 to -25‰ of $\delta^{13}C$ (ref. 14). Values for air[14] are represented by the black square. Arrows show mixing lines between mantle and air (1) biogenic CO_2 and air (2), and mixtures of mantle/air and biogenic CO_2 (3).

($36.6 \pm 11.0\,g\,m^{-2}\,d^{-1}$ and $17.2 \pm 5.0\,g\,m^{-2}\,d^{-1}$, respectively) are higher than background values in graben sediments and uplifted rift lavas (Table 1). The highest individual CO_2 flux measurements (up to $533.5\,g\,m^{-2}\,d^{-1}$) occur along large faults (throws >150 m), which occasionally exhibit aligned hot springs along them (Fig. 3a). Some of these large faults bound the >2-km-deep rift basins[20,21] and are underlain by lower crustal earthquake swarms (Fig. 1).

Diffuse CO_2 flux from tectonic degassing in the Magadi and Natron basin study areas equates to estimated CO_2 outputs of $1.59 \pm 0.53\,Mt\,yr^{-1}$ and $2.46 \pm 1.37\,Mt\,yr^{-1}$, respectively (Table 1) (see Supplementary Information). These values represent tectonic degassing of mantle-derived CO_2 through fault systems away from active volcanic centres, and thus omit CO_2 flux values from volcanoes at the northern (Suswa) and southern (Oldoinyo Lengai) extents of the Magadi–Natron basin. The combined study area represents only ~10% of the entire 9,200 km^2, pervasively faulted basin area; therefore, our flux values represent a conservative minimum estimate for the basin. Despite this cautious approach, the total CO_2 flux from tectonic degassing along fault systems in the Magadi–Natron basin is an order of magnitude greater than the mean diffuse CO_2 flux of reported historically active volcanoes ($0.21\,Mt\,yr^{-1}$; ref. 1; Supplementary Fig. 3). We acknowledge, however, that diffuse CO_2 flux occurs passively over wide areas, and thus CO_2 contributions from diffuse degassing at many volcanoes may be underestimated as a result of sparse sampling and the large study areas required to accurately constrain the flux.

CO_2 is extracted from the mantle by the generation and ascent of magma. It exsolves from magma during cooling, crystallization and decompression. Where extensional fracture systems exist, as in rift zones, exsolved CO_2 has a permeable network through which it may rise to the surface[1,12,22]. Seismic and magnetotelluric studies provide evidence for volumetrically significant accumulations of magma trapped within the crust and upper mantle beneath the Eastern rift[20,23]. These magma bodies provide the probable source for massive CO_2 emissions. Although CO_2 in the Magadi–Natron basin may in part be sourced by upper crustal dykes[24], the flux of CO_2 is

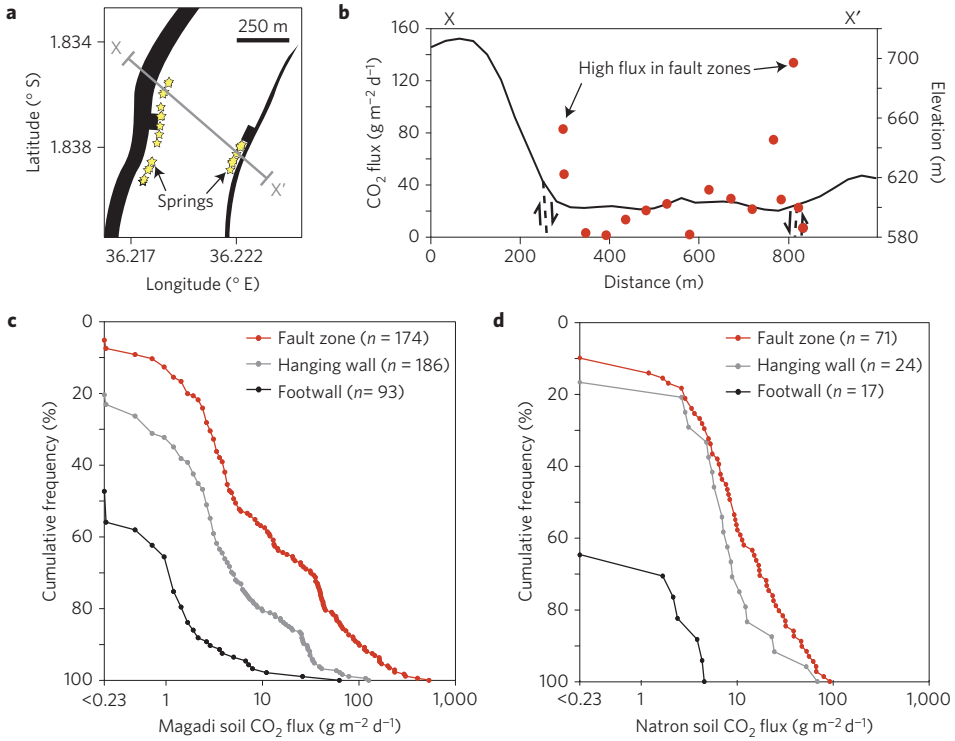

Figure 3 | Summary of CO_2 fluxes throughout the Magadi–Natron basin. a, Simplified structural map of a faulted graben in Magadi basin. Black lines represent faults and yellow stars the location of springs. **b**, Cross-section (X–X′ in **a**) showing the distribution of CO_2 flux (red circles). **c**,**d**, Cumulative frequency plots of diffuse CO_2 flux from all transects across faulted grabens in the study area. Hanging wall represents downthrown sediments, footwalls are uplifted lavas, and fault zones occur adjacent to fault scarps, extending outward on the downthrown side a distance equal to the maximum throw (refer to Supplementary Information).

significant, and requires degassing from the large magma volumes in the crust and mantle (see also Supplementary Information). The association of mantle-derived CO_2 and fault zones provides compelling evidence that CO_2 released from these intrusions into rift-wide fault systems rivals degassing at rift volcanoes. These assertions are further supported by lower crustal earthquakes in the region, which are shown at some rift settings to represent the transport of volatiles exsolved from upper-mantle[12,22] and/or lower-crustal intrusions[25]. Well-located seismicity occurs at depths of 15–27 km (Supplementary Fig. 2) and in some instances can be projected along subsurface border faults[26] (Fig. 1). Steep, rift-parallel zones of lower-crustal to near-surface earthquakes beneath the central Magadi and Natron basins may also mark zones of repeated dyke intrusion within incipient magmatic segments (for example, ref. 23; Fig. 1), providing a potential source for massive CO_2 emissions through rift-wide fault systems.

Although CO_2 flux from tectonic degassing in the Magadi–Natron basin may be higher than other sectors, the growing evidence of CO_2 degassing from even the magma-poor Albertine system[12] suggests the process may apply to other EAR basins. These considerations imply that faults in the EAR probably contribute a significant portion of CO_2 to the global budget. We provide first-order estimates of the total CO_2 flux from tectonic degassing in the Eastern rift using flux measurements from the Magadi–Natron basin (see also Supplementary Information). The ~184 × 50 km Magadi–Natron basin emits a minimum of 4.05 ± 1.90 Mt yr^{-1} of diffuse CO_2 over its areal extent (Table 1), equating to a mean 4.4×10^2 t km^{-2} yr^{-1}. If we applied this flux to the 3,240 × 50 km Eastern rift[7], we would obtain a value of 71 ± 33 Mt yr^{-1} of CO_2, which could potentially increase the global flux from natural systems (637 Mt yr^{-1}; ref. 1) by 11% to 708 Mt yr^{-1}. Although this total CO_2 flux represents only degassing along fault systems away from volcanic centres, it is still of the same order as the total CO_2 output from mid-ocean ridges (53–97 Mt yr^{-1}; refs 2,3). The significance of these flux estimates highlights the important contributions of the East African Rift to the deep carbon cycle, as well as the potential role of deeply derived fluids in assisting rift processes more generally (for example, lower crustal faulting; refs 12,26). However, further diffuse CO_2 surveys across fault systems in Tanzania, Kenya and Ethiopia are required to test whether our flux estimates can be confidently applied to the entire Eastern rift.

Understanding the causes of atmospheric CO_2 variations over geologic timescales is important for reconstructing Earth's climate. For example, baseline greenhouse conditions of the Cretaceous to early Palaeogene were characterized by 4–8 times higher pCO_2 than the Holocene, requiring a 2–2.8 times increase in global CO_2 input to the atmosphere[27]. The exact cause of this increase is poorly constrained, although it has been linked previously to increased rates in arc and/or flood basalt volcanism[27,28]. Our CO_2 emission estimates (tens of Mt yr^{-1}) from tectonic degassing in the EAR show that long-lived (>5 Myr) magma-assisted rifting could produce 10^4 Gt Myr^{-1} of CO_2, after an initial spike of ~1 Gt yr^{-1} associated with flood basalt eruptions[29,30]. During the Cretaceous and Palaeogene, widespread flood basalt volcanism and continental breakup events occurred in association with the Greenland (60–53 Ma), Deccan (65–60 Ma), and Parana (138–125 Ma) large igneous provinces[29]. Based on our estimates, each of these rifting events would be the equivalent of doubling current mid-ocean ridge CO_2 emissions and releasing 10^4 Gt Myr^{-1} of greenhouse gases over the lifetime of rifting. Although this may not be sufficient to achieve the required 4–8 times increase in atmospheric CO_2 compared with the Holocene, widespread continental rift formation, similar to the recently proposed ubiquitous continental arc volcanism[27], provides a compelling and previously unquantified source of massive, long-term CO_2 input to the atmosphere.

Methods

Methods and any associated references are available in the online version of the paper.

Received 26 June 2015; accepted 26 November 2015; published online 18 January 2016

References

1. Burton, M. R., Sawyer, G. M. & Granieri, D. Deep carbon emission from volcanoes. *Rev. Mineral. Geochem.* **75**, 323–354 (2013).
2. Marty, B. & Tolstikhin, I. N. CO_2 fluxes from mid-ocean ridges, arcs and plumes. *Chem. Geol.* **145**, 233–248 (1998).
3. Kagoshima, T. *et al*. Sulphur geodynamic cycle. *Sci. Rep.* **5**, 8330 (2015).
4. Pérez, N. M. *et al*. Global CO_2 emission from volcanic lakes. *Geology* **39**, 235–238 (2011).
5. Seward, T. M. & Kerrick, D. M. Hydrothermal CO_2 emission from the Taupo Volcanic Zone, New Zealand. *Earth Planet. Sci. Lett.* **139**, 105–113 (1996).
6. Chiodini, G. *et al*. Carbon dioxide Earth degassing and seismogenesis in central and southern Italy. *Geophys. Res. Lett.* **31**, L07615 (2004).
7. Ebinger, C. J. & Scholz, C. A. in *Tectonics of Sedimentary Basins: Recent Advances* (eds Busby, C. & Azor, A.) Ch. 9 (John Wiley, 2012).
8. Sawyer, G. M., Carn, S. A., Tsanev, V. I., Oppenheimer, C. & Burton, M. R. Investigation into magma degassing at Nyiragongo volcano, Democratic Republic of the Congo. *Geochem. Geophys. Geosyst.* **9**, Q02017 (2008).
9. Brantley, S. L. & Koepenick, K. W. Measured carbon dioxide emissions from Oldoinyo Lengai and the skewed distribution of passive volcanic fluxes. *Geology* **23**, 933–936 (1995).
10. Pasche, N. *et al*. Methane sources and sinks in Lake Kivu. *J. Geophys. Res.* **116**, G03006 (2011).
11. Hutchison, W., Mather, T. A., Pyle, D. M., Biggs, J. & Yirgu, G. Structural controls on fluid pathways in an active rift system: a case study of the Aluto volcanic complex. *Geosphere* **11**, 542–562 (2015).
12. Lindenfeld, M., Rumpker, G., Link, K., Koehn, D. & Batte, A. Fluid-triggered earthquake swarms in the Rwenzori region, East African Rift—evidence for rift initiation. *Tectonophysics* **566**, 95–104 (2012).
13. Chiodini, G. *et al*. Carbon isotopic composition of soil CO_2 efflux, a powerful method to discriminate different sources feeding soil CO_2 degassing in volcanic hydrothermal areas. *Earth Planet. Sci. Lett.* **274**, 372–379 (2008).
14. Lewicki, J. L. & Brantley, S. L. CO_2 degassing along the San Andreas fault, Parkfield, California. *Geophys. Res. Lett.* **27**, 5–8 (2000).
15. Parks, M. M. *et al*. Distinguishing contributions to diffuse CO_2 emissions in volcanic areas from magmatic degassing and thermal decarbonation using soil gas ^{222}Rn–$\delta^{13}C$ systematics: application to Santorini volcano, Greece. *Earth Planet. Sci. Lett.* **377–378**, 180–190 (2013).
16. Sano, Y. & Marty, B. Origin of carbon in fumarolic gas from island arcs. *Chem. Geol.* **119**, 265–274 (1995).
17. Fischer, T. P. *et al*. Upper mantle volatile chemistry at Oldoinyo Lengai volcano and the origin of carbonatites. *Nature* **459**, 77–80 (2009).
18. Darling, W. G., Greisshaber, E., Andrews, J. N., Armannsson, H. & O'Nions, R. K. The origin of hydrothermal and other gases in the Kenya Rift Valley. *Geochim. Cosmochim. Acta* **59**, 2501–2512 (1995).
19. Fischer, T. P. & Chiodini, G. in *The Encyclopedia of Volcanoes* (eds Sigurdsson, H., Houghton, B., McNutt, S., Rymer, H. & Stix, J.) Ch. 45 (Academic, 2015).
20. Birt, C. S. *et al*. The influence of pre-existing structures on the evolution of the southern Kenya rift valley—evidence from seismic and gravity studies. *Tectonophysics* **278**, 211–242 (1997).
21. Foster, A., Ebinger, C., Mbede, E. & Rex, D. Tectonic development of the northern Tanzanian sector of the east African rift system. *J. Geol. Soc.* **154**, 689–700 (1997).
22. Reyners, M., Eberhart-Phillips, D. & Stuart, G. The role of fluids in lower-crustal earthquakes near continental rifts. *Nature* **446**, 1075–1079 (2007).
23. Keranen, K., Klempere, S. & Gloaguen, R. EAGLE Working Group, Three dimensional seismic imaging of a proto-ridge axis in the Main Ethiopian Rift. *Geology* **39**, 949–952 (2004).
24. Calais, E. *et al*. Aseismic strain accommodation by slow slip and dyking in a youthful continental rift, East Africa. *Nature* **456**, 783–787 (2008).
25. Keir, D. *et al*. Lower crustal earthquakes near the Ethiopian rift induced by magmatic processes. *Geochem. Geophys. Geosyst.* **10**, Q0AB02 (2009).
26. Albaric, J., Déverchère, J., Perrot, J., Jakovlev, A. & Deschamps, A. Deep crustal earthquakes in North Tanzania, East Africa: interplay between tectonic and magmatic processes in an incipient rift. *Geochem. Geophys. Geosyst.* **15**, 374–394 (2014).
27. Lee, C.-T. A. *et al*. Continental arc–island arc fluctuations, growth of crustal carbonates, and long-term climate change. *Geosphere* **9**, 1–36 (2013).

28. Kidder, D. L. & Worsley, T. R. Phanerozoic Large Igneous Provinces (LIPs), HEATT (Haline Euxinic Acidic Thermal Transgression) episodes, and mass extinctions. *Palaeogeogr. Palaeoclimatol. Palaeoecol.* **295**, 162–191 (2010).
29. Courtillot, V., Jaupart, C., Manighetti, I., Tapponnier, P. & Besse, J. On causal links between flood basalts and continental breakup. *Earth Planet. Sci. Lett.* **166**, 177–195 (1999).
30. Self, S., Widdowson, M., Thordarson, T. & Jay, A. E. Volatile fluxes during flood basalt eruptions and potential effects on the global environment: a Deccan perspective. *Earth Planet. Sci. Lett.* **248**, 518–532 (2006).

Acknowledgements

This work was funded by the NSF EAR Tectonics Program, grant numbers 1113066 (T.P.F.), 1113355 (C.J.E.), and 1113677 (S.A.K.). Additional support was provided by Fulbright New Zealand (J.D.M.). CNRS and INSU-supported CoLIBREA project (C.J.E.). We thank the Tanzania COSTECH and the Kenyan National Council for Science and Technology for granting research permits. We acknowledge M. Songo and the Nelson Mandela African Institute of Science and Technology for support. Aerial photographs were provided by the Polar Geospatial Center, University of Minnesota. Aster GDEM is a product of METI and NASA. We gratefully acknowledge support from the Center for Stable Isotopes, UNM. We thank N. Thomas, S. Goldstein, K. Lehnert, B. Onguso, M. Maqway, K. Kimani and the Masai people for help during fieldwork, and A. Van Eaton for helpful comments. We also thank A. Weinstein for earthquake depth analyses, and N. Thomas for entering the geochemical data into the IEDA EarthChem Library.

Author contributions

H.L., J.D.M., T.P.F. and S.A.K. planned the field campaign to the Magadi–Natron basin; H.L., J.D.M., T.P.F., C.J.E. and G.K. carried out the field work; H.L., J.D.M., T.P.F. and G.K. conducted CO_2 flux measurement and collected gas samples; H.L. carried out gas chemistry and carbon isotope analyses; J.D.M. and S.A.K. performed fault analyses to estimate total CO_2 flux; C.J.E. analysed broadband seismic data; Z.D.S. supported carbon isotope analyses at the Center for Stable Isotopes, University of New Mexico; H.L., J.D.M., T.P.F., C.J.E. and S.A.K. collaboratively wrote the paper.

Additional information

Supplementary information is available in the online version of the paper. Reprints and permissions information is available online at www.nature.com/reprints. Correspondence and requests for materials should be addressed to H.L.

Competing financial interests

The authors declare no competing financial interests.

Methods

CO_2 gas accumulation chamber method. The diffuse CO_2 flux survey was performed using the accumulation chamber method described in detail by ref. 31. We used an EGM-4 CO_2 Gas Analyzer (PP Systems), which has a cylindrical chamber with a volume of 1.18×10^{-3} m^3, and an infrared gas analyser with a measurement range of 0–30,000 ppm and <1% error. For each field measurement, the accumulation chamber was pressed firmly into the ground (~2 cm deep) to form a tight seal. Diffuse CO_2 flux was then calculated in the field based on changes in CO_2 concentration (ppm) through time over a 120 s time period.

Field sampling strategy. Owing to the large number of fault systems and eruptive centres in the 184 km-long, 50 km-wide Magadi–Natron basin system, we employed a modified version of the dense grid sampling approach for small sample areas (1–20 km^2; refs 13,32). In contrast to these studies, our analyses focused on understanding CO_2 flux with respect to the location of visible faults (see also Supplementary Information). Where access allowed, CO_2 flux measurements were taken along 500–4,000 m-long transects either parallel or perpendicular to fault strike, with sample spacing varying between 20 and 200 m depending on the length of the transect. In addition to targeting faults, broad transects (4,000–20,000 m long) were taken across the Magadi and Natron basins, with sample spacing between 400 and 4,000 m. In total, 565 flux measurements were taken over the 960 km^2 survey area during 18 days of field work in June and July, 2014.

Laboratory analyses of gas compositions and C isotopes. We collected 115 gas samples, each with an accompanying duplicate sample, for isotope analyses in the Magadi–Natron basin and on Oldoinyo Lengai volcano (Supplementary Table 1 in Supplementary Information). CO_2 concentrations and $\delta^{13}C$ values were assessed using the method of ref. 15. A T-shaped connector, attached to the gas analyser, was used to divert gas into pre-evacuated Labco 12 ml Borosilicate Vials during flux measurements. CO_2 concentrations in the vials were determined at the University of New Mexico (UNM) by a Gow-Mac series G-M 816 Gas Chromatograph (GC) and a Pfeiffer Quadrupole Mass Spectrometer (QMS), which has a mass range from 0 to 120 AMU. The Volcanic and Geothermal Fluid Analysis Laboratory (UNM) has a combination system of GC and QMS that enables measurement of gas species at the same time. Relative abundances of CO_2, CH_4, H_2, $Ar + O_2$, N_2, and CO in the vials were measured on the GC using a He carrier gas. Gas species were separated on the GC using a Hayes Sep pre-column and 5 Å molecular sieve columns. A discharge ionization detector was used for CO_2, CH_4, H_2, $Ar + O_2$, N_2 and CO, respectively[33]. He, Ar, O_2, and N_2 in the vials were also analysed for their relative abundances on the QMS with a secondary electron multiplier detector in dynamic mode. These data were processed using the Quadstar software, which corrects possible mass interferences[34]. Combining the data from GC and QMS, the relative abundances of CO_2, CH_4, H_2, Ar, O_2, N_2 and CO were acquired (see Supplementary Information). Our $\delta^{13}C$-CO_2 values were measured by Isotope Ratio Mass Spectrometer (Finnigan Delta XL) with a gas bench and auto-sampler at the Center for Stable Isotopes, UNM (see Supplementary Information). The $\delta^{13}C$-CO_2 values are presented as per mil (‰) against the standard, Pee Dee belemnite (PDB). Only $\delta^{13}C$-CO_2 values that have higher peak amplitudes of mass 44 (906–10,111 mV) than blank tests (average of 805 mV) were taken. Using the Oztech isotope ratio reference gas, the standard error of analyses is ±0.2‰ (1σ). All reported CO_2 data are presented in the main text and Supplementary Information.

Analysis of broadband seismic data. Continuous waveforms from the 38-station CRAFTI (Continental Rifting in Africa: Fluid-Tectonic Interaction) broadband seismic array and GEOFON stations KMBO and KIBK in Kenya were analysed using the Seismic Handler Motif (SHM) program[35] (Supplementary Fig. 1). P- and S-wave arrival times were picked manually on Butterworth filtered (1–10 Hz) vertical and horizontal components. P phase arrival times were assigned quality factors of 0, 1, 2 or 3 according to estimated measurement errors of 0.05 s, 0.1 s, 0.15 s, and 0.3 s, respectively. S-wave quality factors of 0, 1, 2, and 3 were assigned to arrivals with estimated measurement errors of 0.1 s, 0.175 s, 0.25 s, and 0.3 s, respectively. Only events with a minimum of 6 phases, including at least 3 P-arrivals, were used in the locations; most events had 20 or more phases. The initial locations of earthquakes were found assuming the local velocity model of ref. 36 and using a hypoinverse absolute location algorithm[37]. Progressive GPS timing failures at 32 sites led to changing the network in January and February 2013 and then a gap between March and January 2014. Data used in this study (3,274 events) span 13 January–28 February 2013, and 15 December 2013 to 1 November, 2014. Excluding a few mine blast events and earthquakes at Oldoinyo Lengai volcano, earthquakes are tectonic with impulsive P- and S-arrivals and peak frequencies >5 Hz. Earthquakes presented along profiles A–A′ and B–B′ represent a small, representative proportion of Magadi–Natron data set, consistent with depth histograms of all Natron and Magadi basin earthquakes, which show significant populations at depths between 15 and 27 km (Supplementary Fig. 2). A subset of these earthquakes was relocated using a 3D tomography model of the study area[38]. Depth histograms for earthquakes in the Natron and Magadi basins (excluding Gelai volcano) and those relocated from the 3D tomography model show no systematic variations (Supplementary Fig. 2). The same earthquakes were relocated using the double difference algorithm of ref. 39. Double difference locations for earthquakes along A–A′ and B–B′ have formal position errors of ≤1.5 km and depth errors ≤3.9 km determined by singular value decomposition (errors increase with depth), with additional but small errors associated with 3D velocity variations. Local magnitudes range between 1 and 4.5.

Data availability. The locations, compositions, C isotope values, and structural divisions of measured gas samples from the studied areas are available in Supplementary Information or URL: http://dx.doi.org/10.1594/IEDA/100561.

References

31. Chiodini, G., Cioni, R., Guidi, M., Raco, B. & Marini, L. Soil CO_2 flux measurements in volcanic and geothermal areas. *Appl. Geochem.* **13**, 543–552 (1998).
32. Werner, C. & Cardellini, C. Comparison of carbon dioxide emissions with fluid upflow, chemistry, and geologic structures at the Rotorua geothermal system, New Zealand. *Geothermics* **35**, 221–238 (2006).
33. Giggenbach, W. F. & Goguel, R. L. *Methods for The Collection and Analysis of Geothermal and Volcanic Water and Gas Samples* Tech. Rep. CD2401 (Department of Scientific and Industrial Research, Institute of Geological and Nuclear Sciences, New Zealand, 1989).
34. de Moor, J. M. *et al*. Gas chemistry and nitrogen isotope compositions of cold mantle gases from Rungwe Volcanic Province, southern Tanzania. *Chem. Geol.* **339**, 30–42 (2013).
35. Stammler, K. SeismicHandler—programmable multichannel data handler for interactive and automatic processing of seismological analysis. *Comp. Geosci.* **19**, 135–140 (1993).
36. Albaric, J. *et al*. Contrasted seismogenic and rheological behaviours from shallow and deep earthquake sequences in the North Tanzanian Divergence, East Africa. *J. Afr. Earth Sci.* **58**, 799–811 (2010).
37. Klein, F. W. *Hypocenter Location Program HYPOINVERSE* Tech. Rep. 78-698 (US Geological Survey, 1978).
38. Roecker, S. *et al*. *Images of the East Africa Rift System from the Joint Inversion of Bodywaves, Surfacewaves, and Gravity: Investigating the Role of Magma in Early-stage Continental Rifting* Am. Geophys. Union Fall Meeting T51G-3013 107 (AGU, 2015).
39. Waldhauser, F. & Ellsworth, W. A double-difference earthquake location algorithm: method and application to the northern Hayward fault, California. *Bull. Seismol. Soc. Am.* **90**, 1353–1368 (2000).